EMD-seislet transform[a]

[a]Published in Geophysics, 83, A27-A32, (2018)

Yangkang Chen and Sergey Fomel†*

ABSTRACT

The seislet transform uses a prediction operator which is connected to the local slope or frequency of seismic events. In this paper, we propose combining the 1D non-stationary seislet transform with empirical mode decomposition (EMD) in the $f-x$ domain. We use the EMD to decompose data into smoothly variable frequency components for the following 1D seislet transform. The resultant representation shows remarkable sparsity. We introduce the detailed algorithm and use a field example to demonstrate the application of the new seislet transform for sparsity-promoting seismic data processing.

INTRODUCTION

Sparse approximation aims at extracting the most important information of the given data by a linear combination of pre-specified atom signals with sparse linear coefficients. Sparse approximation theory has been a rapidly evolving field in digital image analysis, since many state-of-the-art signal and image processing tasks have been successfully handled with the concept of sparsity, including image inpainting and restoration (Elad et al., 2005; Mairal et al., 2008, 2009; Cai et al., 2013), image denoising (Protter and Elad, 2009; Cai et al., 2013), data compression (Bryt, 2008), blind source separation (Zibulevsky and Pearlmutter, 2001), etc.

Over the past several decades, different types of sparse transforms have been explored for seismic data processing applications, and promising results have been reported. LePennec and Mallat (1992) applied a wavepacket transform to seismic data compression. Zhang and Ulrych (2003) developed a type of wavelet frame that takes into account the characteristics of seismic data both in time and space for denoising applications. Ioup and Ioup (1998) applied wavelet transform to both random noise removal and data compression with soft thresholding in the wavelet domain. Du and Lines (2000) applied multi-resolution property of wavelet transform to attenuate tube waves. Jafarpour et al. (2009) used a discrete cosine transform (DCT) to obtain sparse representations of fields with distinct geologic features and improve the solutions to traditional geophysical estimation problems. A number of researchers have also reported successful applications of the curvelet transform (Candès et al., 2006) in different seismic data processing tasks thanks to the multi-scale and sparse property of the curvelet domain (Hennenfent and Herrmann, 2006;

Wang et al., 2008).

Fomel and Liu (2010) introduced a data-adaptive sparsity promoting transform, called the *seislet* transform. Following the lifting scheme used in the construction of second-generation digital wavelets (Sweldens, 1995), the seislet transform utilizes the spatial predictability property of seismic data to construct the predictive operator. Fomel and Liu (2010) used plane-wave construction (PWD) to aid the prediction process. Instead of using PWD, Liu and Fomel (2010) used differential offset continuation (OC) to construct seislet transform for pre-stack reflection data. OC-seislet transform can obtain better sparsity for conflicting-dip pre-stack seismic data in that OC seislet uses offset continuation (Fomel, 2003) instead of local slopes to connect different common offset gathers. In order to relieve the dependence of seislet transform on local slope estimation, Liu and Liu (2013) and Liu et al. (2015) proposed a velocity-dependent (VD) seislet transform based on conventional velocity analysis. The seislet transform has also found a recent application in simultaneous-source separation (Chen et al., 2014a). Instead of using a single slope or frequency map to sparsify the seismic data, Fomel and Liu (2010) proposed to apply several seislet transforms with smoothly variable slopes or frequencies, which are referred to as seislet frames.

Empirical mode decomposition (EMD) is a recently popular signal processing method (Huang et al., 1998), which was proposed to prepare a stable input for the Hilbert transform. The essence of EMD is to stabilize a highly non-stationary signal by decomposing it into smoothly variable frequency components, which are called intrinsic mode functions (IMF). EMD has found many successful applications in seismic data processing, such as time-frequency analysis (Han and van der Baan, 2013) and noise attenuation (Bekara and van der Baan, 2009; Chen and Ma, 2014; Chen et al., 2014b, 2015).

In this paper, we propose to use EMD to create sparse transforms for representing seismic data. We first transform the input seismic data from $t-x$ domain to $f-x$ domain, then apply EMD to each frequency slice to decompose input data into smoothly variable frequency components. Next, 1D non-stationary seislet transform is applied independently to each component. We evaluate the sparsity of the new representation (EMD-seislet transform) and apply it to noise attenuation of a seismic image.

METHOD

Empirical mode decomposition

The process of EMD has the following simple expression:

$$s(t) = \sum_{n=1}^{N} c_n(t) + r(t), \tag{1}$$

where $s(t)$ is the original non-stationary signal, $c_n(t)$ $(n = 1, 2, \cdots, N)$ denotes each separated IMF, N denotes the number of separated IMF, and $r(t)$ denotes the residual after EMD. The process of EMD is to gradually remove the stable oscillations embedded in the original signal to arrive at a monotonic and smooth residual or trend at last. A special property of the EMD is that the IMFs represent different oscillations embedded in the data, where the oscillating frequency for each sub-signal $c_n(t)$ decreases with IMF order increasing (Huang et al., 1998).

1D seislet transform

The seislet transform can be constructed by multi-scale prediction of the odd components **o** from the even components **e**:

$$\mathbf{r} = \mathbf{o} - \mathbf{P}(\mathbf{e}), \tag{2}$$
$$\mathbf{c} = \mathbf{e} + \mathbf{U}(\mathbf{r}). \tag{3}$$

In the above equations, **P** denotes the prediction operator and **U** denotes the updating operator at a particular scale. **r** denotes the difference vector and **c** denotes the updated even component. The inverse seislet transform follows the inverse process of equations 2 and 3 continuing from large to small scale. The difference between the 1D seislet transform and the 1D wavelet transform is whether the prediction is modulated by an appropriate frequency. In the simplest case of Haar transform, the Z-transform domain prediction filter for the Haar wavelet transform is

$$P(Z) = Z, \tag{4}$$

and the Z-transform domain Haar prediction filter for wavelet transform is

$$U(Z) = Z/2. \tag{5}$$

However, for the seislet transform,

$$P(Z) = Z/Z_0, \tag{6}$$
$$U(Z) = 1/2(Z/Z_0). \tag{7}$$

where $Z_0 = e^{i\omega_0 \Delta t}$. The prediction filter in equation 6 can perfectly characterize a sinusoid with ω_0 angular frequency sampled on a Δt grid. Analogously, the prediction filter for biorthogonal 2/2 transform can be expressed as:

$$P(Z) = 1/2(Z/Z_0 + Z_0/Z), \tag{8}$$

and its corresponding updating operator is

$$U(Z) = 1/4(Z/Z_0 + Z_0/Z). \tag{9}$$

1D non-stationary seislet transform

When a 1D signal has a constant angular frequency, the prediction filter in equation 6 can characterize a sinusoidal signal. When the 1D signal contains a sinusoid with a variable frequency, or in other words, is non-stationary, we can replace Z_0 with Z_t, $Z_t = e^{i\omega(t)\Delta t}$ denotes the frequency modulation at time t. Let us modify equation 8 to the following form:

$$P_t(Z) = 1/2(Z/Z_t + Z_t/Z), \tag{10}$$

in order to best characterize the non-stationary signal. $P_t(Z)$ denotes the prediction filter at time t. In the physical domain, the linear prediction and updating operators can be expressed as:

$$P_t(e) = (S_t^{(+)}(e_{t-1}) + S_t^{(-)}(e_t))/2, \tag{11}$$

$$U_t(r) = (S_t^{(+)}(r_{t-1}) + S_t^{(-)}(r_t))/4, \tag{12}$$

where $S_t^{(+)}$ and $S_t^{(-)}$ are operators that predict an element from its left and right neighbors by modulating each element according to their local frequency $\omega(t)$.

Figure 1 shows a comparison between the wavelet transform and the 1D stationary and non-stationary seislet transforms in compressing a 1D signal with smooth frequency components. The frequency ranges from 250 to 186 Hz. Both the wavelet transform and stationary seislet transform fail to compress the signal well while the non-stationary seislet transform obtains a perfectly sparse representation.

Estimating local frequency by complex non-stationary autoregression

According to the autoregressive spectral analysis theory (Marple, 1987), a complex time series that has a constant frequency component is predictable by a two-point prediction-error filter $(1, -e^{i\omega_0\Delta t})$. Suppose a complex time series is $d(t)$. In Z-transform notation, the two-point prediction-error filter can be expressed as:

$$F(Z) = 1 - Z/Z_0. \tag{13}$$

We assume that a 1D time series has a smooth frequency component, then the 1D time series can be locally predicted using different local two-point prediction-error filters $(1, -e^{i\omega(t)\Delta t})$:

$$d(t) = e^{i\omega(t)\Delta t} d(t - \Delta t). \tag{14}$$

In order to estimate $\omega(t)$ using equation 14, we need to first minimize the least-squares misfit of the true and predicted time series with a local-smoothness constraint:

$$\min_{\mathbf{a}} \parallel \mathbf{d} - \mathbf{D}\mathbf{a} \parallel_2^2 + \mathbf{R}(\mathbf{a}), \tag{15}$$

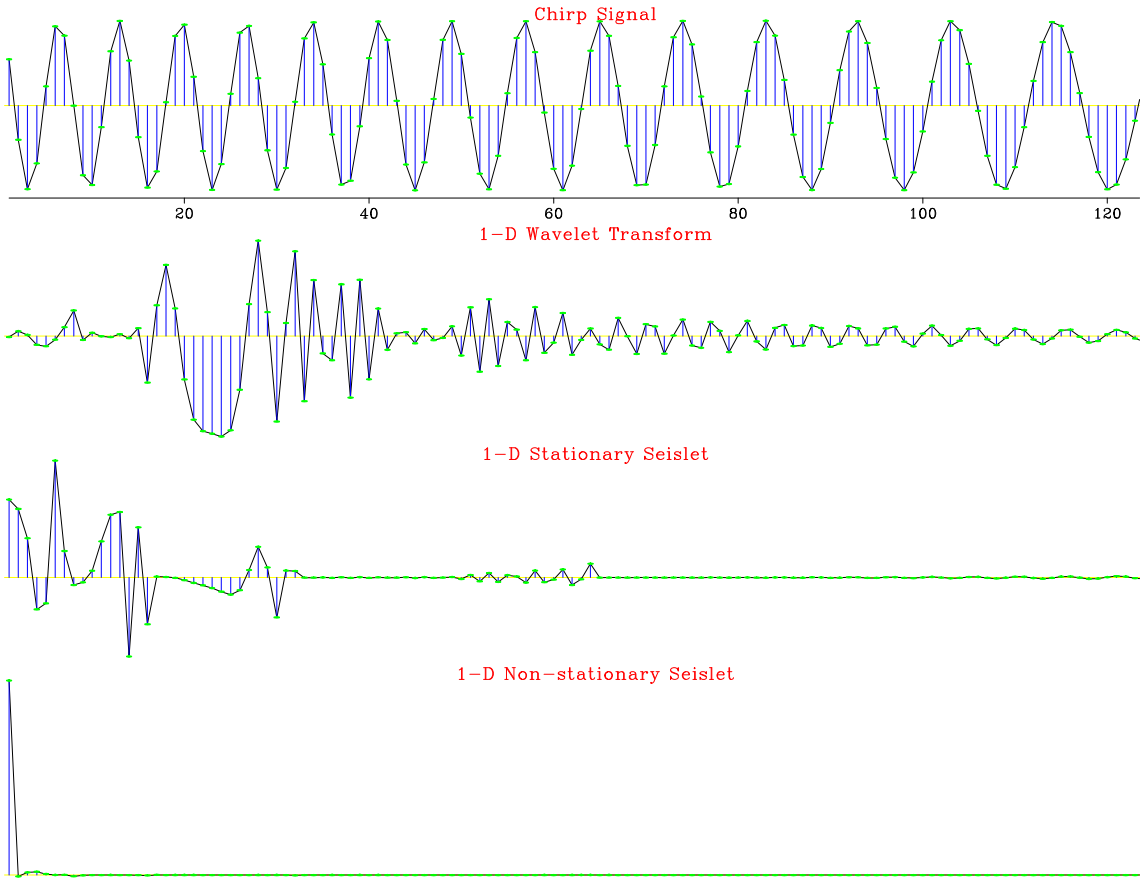

Figure 1: Demonstration of 1D non-stationary seislet transform for non-stationary signal. Upper: non-stationary chirp signal, frequency ranges from 250 to 186 Hz. Upper middle: compressed using 1D wavelet transform. Down middle: compressed using 1D stationary seislet transform with the frequency of 250 Hz. Down: compressed using 1D non-stationary seislet transform.

where $\mathbf{d}$ and $\mathbf{a}$ are vectors composed of the entries $d(t)$ and $a(t)$, respectively, and $a(t) = e^{i\omega(t)\Delta t}$. $\mathbf{D}$ is a diagonal matrix composed of the entries $d(t-\Delta t)$. $\mathbf{R}$ denotes the local-smoothness constraint. Equation 15 can be solved using shaping regularization:

$$\hat{\mathbf{a}} = [\lambda^2\mathbf{I} + \mathcal{T}(\mathbf{D}^T\mathbf{D} - \lambda^2\mathbf{I})]^{-1}\mathcal{T}\mathbf{D}^T\mathbf{d}, \tag{16}$$

where $\mathcal{T}$ is a triangle smoothing operator and λ is a scaling parameter that controls the physical dimensionality and enables fast convergence. λ can be chosen as the least-squares norm of $\mathbf{D}$. After the filter coefficient $a(t)$ is obtained, we can straightforwardly calculate the local angular frequency $\omega(t)$ by

$$\omega(t) = Re\left[\frac{\arg(a(t))}{\Delta t}\right]. \tag{17}$$

Preparing smoothly variable frequency components by EMD

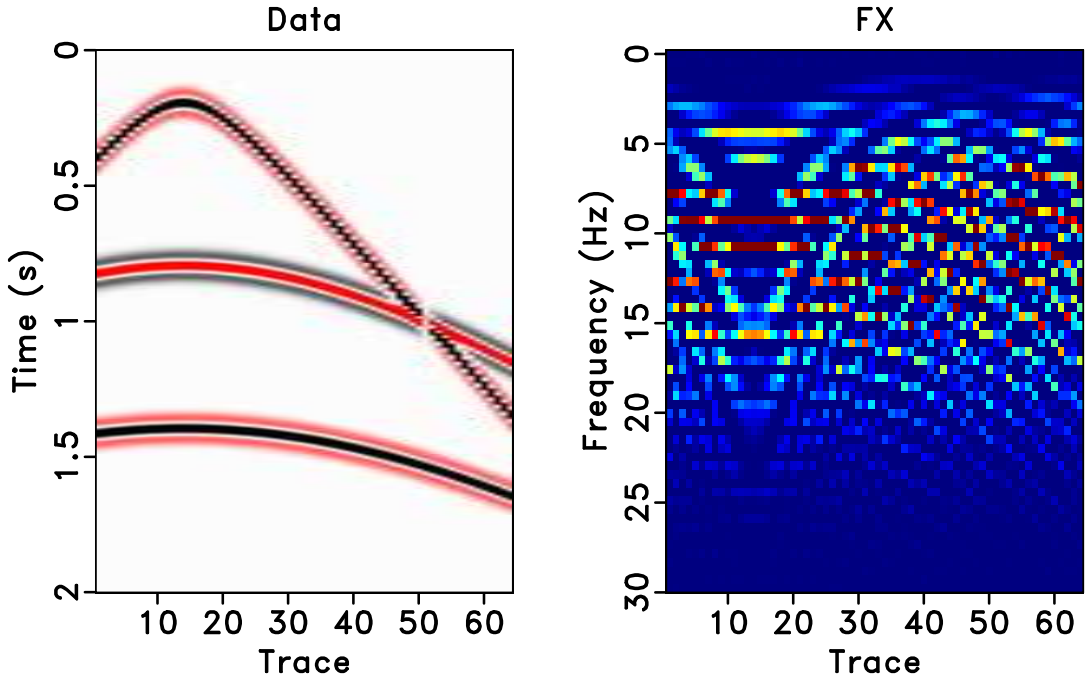

(a) (b)

Figure 2: (a) Synthetic example with hyperbolic events. (b) $f - x$ spectrum of (a).

The aforementioned 1D non-stationary seislet transform adapts to 1D signals that have smoothly variable frequency components since its compression performance is controlled by the predicting and updating procedures between the series elements according to a locally smooth modulation frequency. Correspondingly, when calculating the local frequency, we also assume the 1D signal to have smoothly variable frequency components.

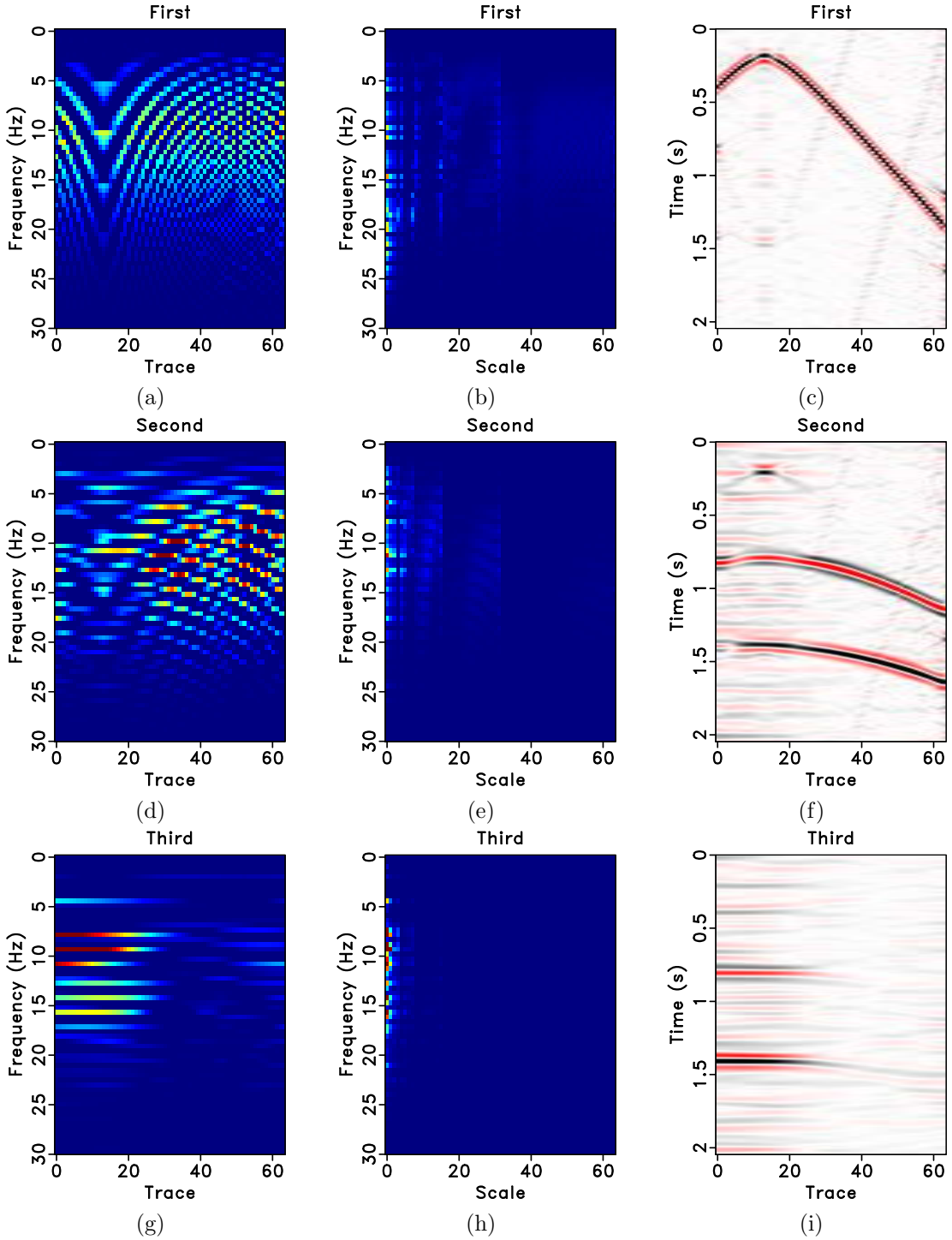

Figure 3: A demonstration of the EMD-seislet transform. The left column shows the decomposed $f-x$ domain spectrum using EMD. The middle column shows the compressed $f-x$ domain using 1D non-stationary seislet transform. The right column shows the reconstructed $t-x$ domain data corresponding to different components.

We call the combined FFT-EMD-seislet workflow the *EMD-seislet* transform. Figures 2 and 3 provide a detailed demonstration of the procedures involved in the EMD-seislet transform construction. Figure 2a shows a synthetic data with hyperbolic events. Figure 2b shows the $f-x$ spectrum of the synthetic data. Figure 4 shows a demonstration for preparing smoothly variable frequency components for each frequency slice using the EMD in the $f-x$ domain. We can observe that each frequency slice in the $f-x$ domain is highly non-stationary. After EMD decomposition, the three decomposed $f-x$ domain components are shown in the left column of Figure 3. Each component now has smoothly non-stationary frequency slices. After 1D non-stationary seislet transforms, the three $f-x$ domain components become highly compressed. The middle column in Figure 3 shows the compressed $f-x$ domain using the 1D non-stationary seislet transform. The scale of the compressed coefficients is indicated by the horizontal axis. The right column in Figure 3 shows the reconstructed $t-x$ domain data from the decomposed and compressed components in the middle column. The three decomposed components correspond to different parts of the input signal.

In order to compare the sparsity in compressing seismic data, we plot the reconstruction error curves with respect to the number of selected largest coefficients. The reconstruction error is defined as $E = \| \mathbf{d} - \mathbf{A}\mathbf{m}_N \|_2^2$, where $\mathbf{m}_N$ denotes the largest N coefficients in the transform domain. The faster the curve decays, the sparser the corresponding transform domain will be. As shown in Figure 5, the EMD-seislet appears to be the sparsest compared with the PWD-seislet transform, wavelet transform, and Fourier transform.

APPLICATION OF NOISE ATTENUATION TO REAL DATA

We use a real data example shown in Figure 6a to demonstrate the performance of the proposed EMD-seislet in attenuating random noise. Figure 6c shows the denoised result by thresholding in the EMD-seislet transform domain. Figure 6d shows the removed noise section using EMD-seislet thresholding. 2% of EMD-seislet coefficients were retained. Despite the complicated structures of the seismic image, the proposed approach obtains a successful denoising performance. Figure 6f shows the denoised result using the traditional seislet thresholding method. Figure 6i shows the denoised result using the FX Decon method. Figures 6g and 6j show the removed noise corresponding to the seislet thresholding method and the FX Decon method, respectively. Figures 6b, 6e, 6h, and 6k show the enlarged sections (corresponding to the frame boxes in Figure 6). From the comparison in Figure 6 the proposed approach obtains the best result, while the seislet thresholding is over-smoothing, and the FX Decon harms some of the signal energy. The over-smoothing effect of the seislet thresholding method may be due to the over-smooth local slope calculated using the PWD algorithm. The signal-leakage problem of the FX Decon method has been widely studied in the literature, e.g., in Chen and Ma (2014). The EMD-seislet domains

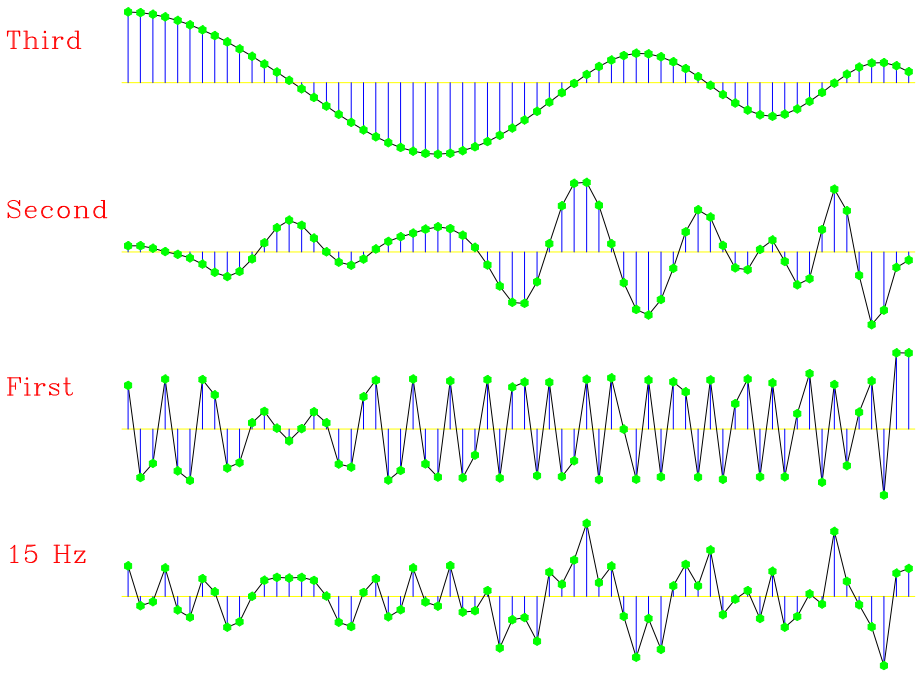

Figure 4: Demonstration of preparing the smoothly variable frequency components by EMD for the 15 Hz slice of the synthetic data in Figure 2a.

before and after applying the thresholding operator are plotted in Figures 7a and 7b, respectively. It is clear that the thresholding removes most low-amplitude coefficients in the sparse EMD-seislet domain.

CONCLUSIONS

We have proposed a novel approach for sparsifing seismic data: EMD-seislet transform. The approach relies on the ability of empirical mode decomposition (EMD) in the $f-x$ domain to provide smoothly non-stationary data, which we use in the following 1D non-stationary seislet transform. When applied to seismic data with multiple conflicting slopes, EMD-seislet is remarkably sparse. A real data example shows an excellent performance of the EMD-seislet transform in attenuating random noise. However, the large computational cost required by the EMD algorithm requires a careful design of the parallel computing framework in the future research.

ACKNOWLEDGMENTS

We appreciate the comments from three anonymous reviewers that greatly improved the manuscript.

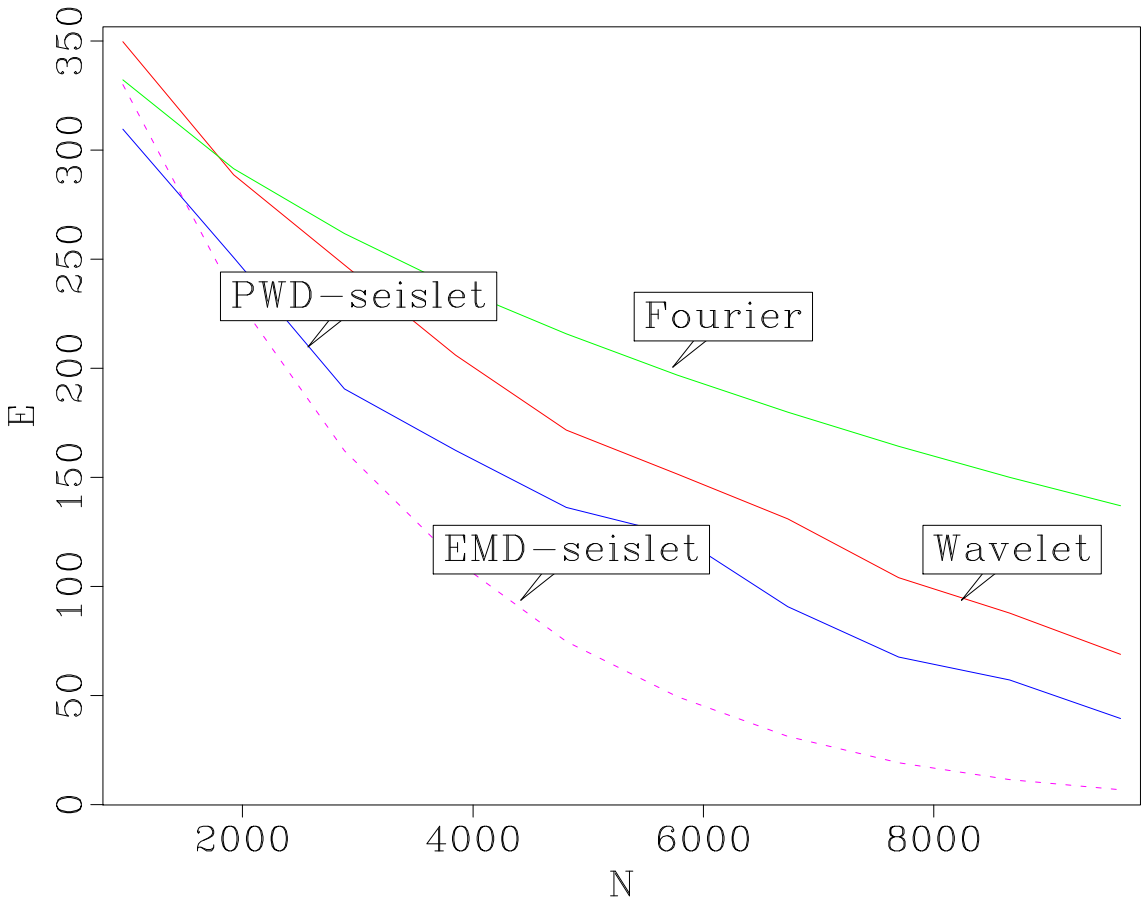

Figure 5: Sparsity comparison. $E = \| \mathbf{d} - \mathbf{A}\mathbf{m}_N \|_2^2$ denotes the reconstruction error with the largest N coefficients in the transform domain.

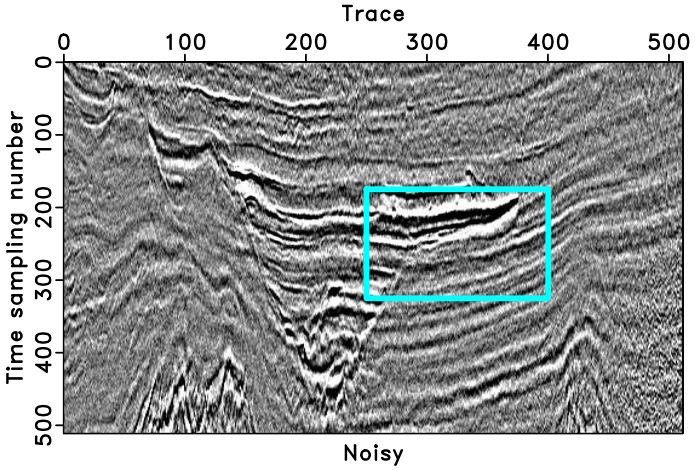
Trace
0
100
200
300
400
500
Time sampling number
0
100
200
300
400
500
Noisy

(a)

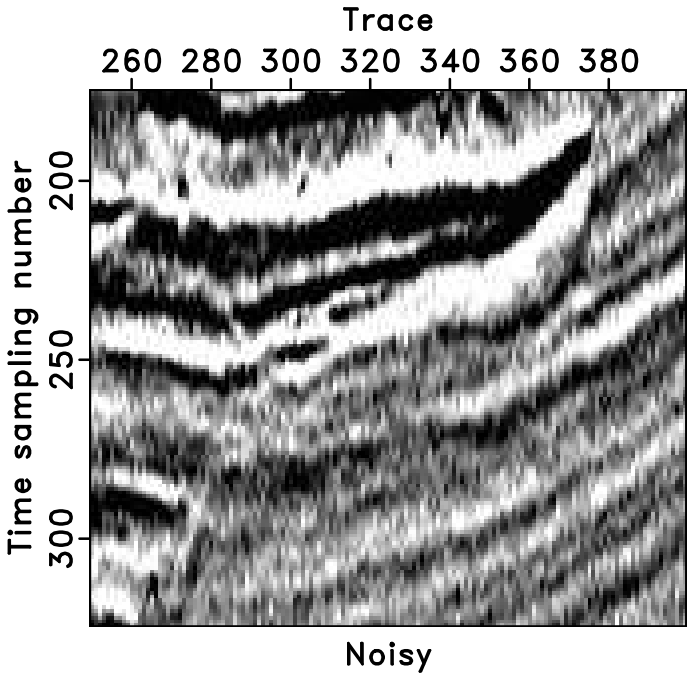
Trace
260
280
300
320
340
360
380
Time sampling number
200
250
300
Noisy

(b)

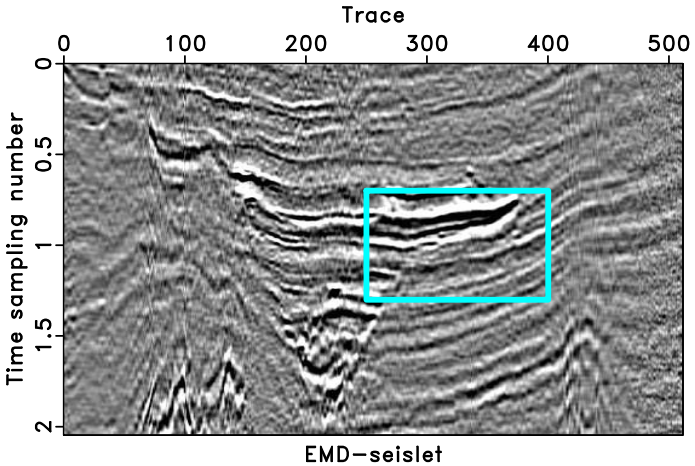
Trace
0
100
200
300
400
500
Time sampling number
0
0.5
1
1.5
2
EMD−seislet

(c)


Trace
0
100
200
300
400
500

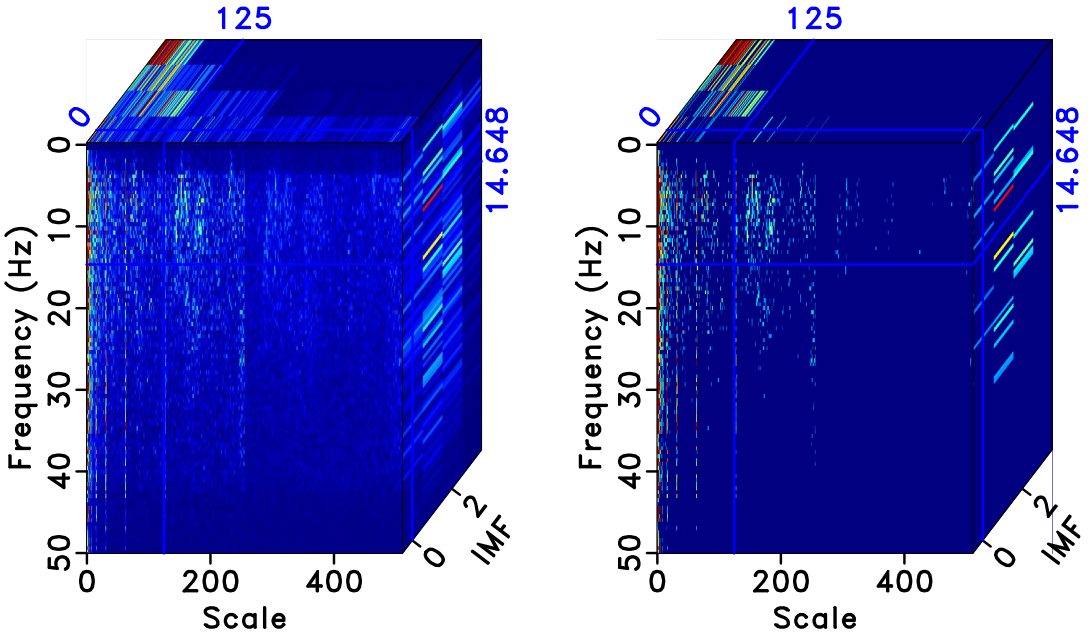

(a) (b)

Figure 7: (a) EMD-seislet domain before thresholding. (b) EMD-seislet domain after thresholding.

REFERENCES

Bekara, M., and M. van der Baan, 2009, Random and coherent noise attenuation by empirical mode decomposition: Geophysics, **74**, V89–V98.

Bryt, O., 2008, Compression of facial images using the K-SVD algorithm: Journal of Visual Communication and Image Representation, **19**, 270–283.

Cai, J., S. Huang, H. Ji, Z. Shen, and G. Ye, 2013, Data-driven tight frame construction and image denoising: Applied and Computational Harmonic Analysis, doi: 10.1016/j.acha.2013.10.001.

Candès, E. J., L. Demanet, D. L. Donoho, and L. Ying, 2006, Fast discrete curvelet transforms: SIAM, Multiscale Modeling and Simulation, **5**, 861–899.

Chen, Y., S. Fomel, and J. Hu, 2014a, Iterative deblending of simultaneous-source seismic data using seislet-domain shaping regularization: Geophysics, **79**, no. 5, V179–V189.

Chen, Y., S. Gan, T. Liu, J. Yuan, Y. Zhang, and Z. Jin, 2015, Random noise attenuation by a selective hybrid approach using f-x empirical mode decomposition: Journal of Geophysics and Engineering, **12**, 12–25.

Chen, Y., and J. Ma, 2014, Random noise attenuation by *f-x* empirical mode decomposition predictive filtering: Geophysics, **79**, V81–V91.

Chen, Y., C. Zhou, J. Yuan, and Z. Jin, 2014b, Application of empirical mode decomposition to random noise attenuation of seismic data: Journal of Seismic Exploration, **23**, 481–495.

Du, B., and L. R. Lines, 2000, Attenuating coherent noise by wavelet transform:

Exploration Geophysics, **31**, 353–358.
Elad, M., J. L. Starck, P. Querre, and D. L. Donoho, 2005, Simultaneous cartoon and texture image inpainting using morphological component analysis (mca): Applied and Computational Harmonic Analysis, **19**, 340–358.
Fomel, S., 2003, Seismic reflection data interpolation with differential offset and shot continuation: Geophysics, **68**, 733–744.
Fomel, S., and Y. Liu, 2010, Seislet transform and seislet frame: Geophysics, **75**, V25–V38.
Han, J., and M. van der Baan, 2013, Empirical mode decomposition for seismic time-frequency analysis: Geophysics, **78**, O9–O19.
Hennenfent, G., and F. Herrmann, 2006, Seismic denoising with nonunformly sampled curvelets: Computing in Science & Engineering, **8**, 16–25.
Huang, N. E., Z. Shen, S. R. Long, M. C. Wu, H. H. Shih, Q. Zheng, N.-C. Yen, C. C. Tung, and H. H. Liu, 1998, The empirical mode decomposition and the Hilbert spectrum for nonlinear and non-stationary time series analysis: Proceeding of the Royal Society of London Series A, **454**, 903–995.
Ioup, J. W., and G. E. Ioup, 1998, Noise removal and compression using a wavelet transform: 68th Annual International Meeting, SEG, Expanded Abstracts, 1076–1079.
Jafarpour, B., V. K. Goyal, D. B. McLaughlin, and W. T. Freeman, 2009, Transform-domain sparsity regularization for inverse problems in geosciences: Geophysics, **74**, R69–R83.
LePennec, E., and S. Mallat, 1992, Sparse geometric image representations with bandelets: 62nd Annual International Meeting, SEG, Expanded Abstracts, 1187–1190.
Liu, Y., and S. Fomel, 2010, OC-seislet: Seislet transform construction with differential offset continuation: Geophysics, **75**, WB235–WB245.
Liu, Y., S. Fomel, and C. Liu, 2015, Signal and noise separation in prestack seismic data using velocity-dependent seislet transform: Geophysics, **80**, no. 6, WD117–WD128.
Liu, Y., and C. Liu, 2013, Velocity-dependent seislet transform and its applications: 83rd Annual International Meeting, SEG, Expanded Abstracts, 3661–3666.
Mairal, J., F. Bach, J. Ponce, G. Sapiro, and A. Zisserman, 2009, Non-local sparse models for image restoration: IEEE 12th International Conference on Computer Vision.
Mairal, J., G. Sapiro, and M. Elad, 2008, Learning multiscale sparse representations for image and video restoration: SIAM Multiscale Modeling Simulation, **7**, 214–241.
Marple, S. L., 1987, Digital spectral analysis with applications: Prentice-Hall.
Protter, M., and M. Elad, 2009, Image sequence denoising via sparse and redundant representations: IEEE Trans Image Process, **18**, 27–35.
Sweldens, W., 1995, Lifting scheme: A new philosophy in biorthogonal wavelet constructions: Wavelet applications in signal and image processing iii: Proceedings of SPIE 2569, 68–79.
Wang, D., R. Saab, O. Yilmaz, and F. J. Herrmann, 2008, Bayesian wavefield separation by transform-domain sparsity promotion: Geophysics, **73**, A33–A38.
Zhang, R., and T. Ulrych, 2003, Physical wavelet frame denoising: Geophysics, **68**,

225–231.

Zibulevsky, M., and B. A. Pearlmutter, 2001, Blind source separation by sparse decomposition in a signal dictionary: Neural computation, **13**, 863–882.